

Shortwave radiation and cloud parameterizations for intermediate complexity models

J.J. Beersma, R. van Dorland and J.D. Opsteegh

*Royal Netherlands Meteorological Institute (KNMI),
P.O. Box 201, 3730 AE De Bilt, The Netherlands*

February 2002

Contents

List of figures	3
1 Introduction	5
2 The intermediate complexity model ECBilt	5
3 Shortwave radiation parameterization	6
3.1 Performance of the shortwave radiation parameterization	9
4 Cloud cover parameterization	11
4.1 Performance of the cloud parameterization in ECBilt	12
4.1.1 Average cloud cover	12
4.1.2 Cloud cover variability	12
5 The ECBilt2 climatology: dynamical versus climatological clouds	13
5.1 Surface temperature	13
5.2 Geopotential height	14
5.3 Diabatic heating	14
5.4 Summary and discussion of the differences	15
6 The ECBilt2 climatology: anomaly versus climatological clouds	15
6.1 Surface temperature	16
6.2 Geopotential height	16
6.3 Diabatic heating	17
6.4 Precipitation	17
6.5 Summary and discussion of the differences	17
7 Discussion and conclusions	18
Acknowledgements	20
References	21
Figures	23

List of Figures

1	Difference between ECHAM4-RTM net absorbed shortwave fluxes at the surface and the parameterized fluxes at the surface for January and July. Left panels: parameterization with one cloud type; right panels: parameterization with 3 cloud types and explicit function on cloud liquid water path (lwp). Units are Wm^{-2}	23
2	Simulated (upper panels) and observed ISCCP total cloud cover for DJF (December–February) and JJA (June–August).	24
3	Simulated (upper panels) and ISCCP inter-monthly standard deviation of cloud cover for DJF and JJA. ISCCP data are smoothed for presentation	25
4	Simulated daily standard deviation of cloud cover for DJF and JJA (upper panels), and ISCCP daily standard deviations for January 1988 and July 1988. ISCCP data are obtained from Chen and Roeckner (1997) and smoothed for presentation.	26
5	Difference in surface temperature ($^{\circ}\text{C}$) between the simulation with dynamical clouds and the simulation with prescribed climatological clouds for DJF and JJA. The lower panels give the corresponding t -values of the differences. t -values larger than 2 or smaller than -2 roughly denote statistically significant differences at the 5%-level (t -test).	27
6	Interannual and daily surface temperature standard deviation ratios of the simulation with dynamical clouds and the simulation with prescribed climatological clouds for DJF (left panels) and JJA (right panels). The results are smoothed using a 9-point filter.	28
7	Geopotential height differences (m) between the simulation with dynamical clouds and the simulation with climatological clouds at 200, 500 and 800 hPa in DJF.	29
8	Difference in daily standard deviation of 200 hPa geopotential height (m) in the simulation with dynamical clouds and the simulation with climatological clouds (upper panel), and daily standard deviation of 200 hPa geopotential height (m) in the climatological cloud simulation (lower panel).	30
9	Diabatic heat differences ($^{\circ}\text{C day}^{-1}$) between the simulation with dynamical clouds and the simulation with climatological clouds for the layer between 500 and 200 hPa (upper panel) and the layer between 1000 and 500 hPa (lower panel) in DJF.	31
10	Interannual and daily surface temperature standard deviation ratios of the anomaly cloud simulation and the climatological cloud simulation for DJF (left panels) and JJA (right panels). The results are smoothed using a 9-point filter.	32
11	Geopotential height differences (m) between the simulation with anomaly clouds and the simulation with climatological clouds for 200, 500 and 800 hPa in DJF.	33

12	Difference in daily standard deviation of 200 hPa geopotential height (m) in the simulation with anomaly clouds and the simulation with climatological clouds (upper panel) and daily standard deviation of 200 hPa geopotential height (m) in the anomaly cloud simulation (lower panel).	34
13	Ratios of standard deviations of diabatic heat in the simulation with anomaly clouds and the simulation with climatological clouds for the layer between 500 and 200 hPa in DJF. Upper panel: interannual standard deviations; bottom panel: daily standard deviations. The results are filtered using a 9-point smoother.	35
14	Interannual and daily precipitation standard deviation ratios of the anomaly cloud simulation and the climatological cloud simulation for DJF (left panels) and JJA (right panels). Precipitation consists of both large scale and convective precipitation. The results are smoothed using a 9-point filter.	36

1 Introduction

Clouds play an important role in the climate system by affecting the Earth's radiation balance. Basically clouds reflect the solar shortwave radiation and they absorb the terrestrial longwave radiation. The reflection and absorption depend on the amount, location, height and type of clouds and on the time of the year. In the global and annual mean, clouds have a cooling effect on the present climate (IPCC, 1996).

The intermediate complexity climate model ECBilt (Haarsma et al., 1996; Opsteegh et al., 1998) has been used for long present-day climate simulations to study the natural variability on decadal to centennial time scales. Due to an implicit treatment of clouds in the radiation parameterization the simulations so far made use of a prescribed climatological cloud distribution. It is reasonable to assume that cloud variability has an influence on the natural variability at various time scales. It is however not clear how relevant cloud variability is for the climate simulations that are performed with ECBilt.

Intermediate complexity models are not only used to study natural variability on longer time scales for which very long climate simulations are needed ($\sim 1000\text{yr}$). Since this type of models is much cheaper to run than current state-of-the-art climate models they are also very useful for doing large numbers of idealized experiments. There is thus clearly a need for efficient parameterizations that include the relevant physical processes.

In this paper two such parameterizations are presented. An efficient shortwave radiation scheme is introduced in which cloud cover is treated explicitly. In addition a simple cloud parameterization is presented. The combination of these parameterizations makes it possible to efficiently incorporate cloud cover variability and cloud cover feedbacks in intermediate complexity models.

The parameterizations are implemented in the intermediate complexity model ECBilt in order to study the effects of dynamical clouds. The second part of this paper is devoted to an analysis of the impact of cloud cover variability on the mean climate of the model and its variability on daily to interannual time scales in comparison to simulations with prescribed climatological clouds.

2 The intermediate complexity model ECBilt

The atmospheric model ECBilt is a spectral quasi-geostrophic model with three vertical levels. The horizontal resolution is truncated at T21. The dynamical part of the model is based on Marshall and Molteni (1993). As an extension, the neglected ageostrophic terms in the vorticity and thermodynamic equations are included as forcings which are diagnostically derived from the vertical motion field. The physical parameterizations contain bulk formulae for the exchange of sensible and latent heat. In the original simple schemes for shortwave and longwave radiation the effects of clouds were prescribed. For solar radiation the reflection and absorption coefficients were a function of latitude and time of the year and thus implicitly depended on clouds. The longwave radiation was parameterized as a function of the vertical

structure of the potential temperature following Held and Suarez (1978). In the parameterization of downward longwave radiation at the surface (after Holtslag and van Ulden, 1983) zonally averaged cloud cover was used. The hydrological cycle is described by an advection equation for moisture. The cycle is closed by river runoff, snow melt and soil moisture. The main characteristics of the model relevant for cloud 'prediction' are given below. Further details about the model are given by Haarsma et al. (1996) and Opsteegh et al. (1998).

For the computation of the diabatic heating the atmosphere is divided in two layers: one between the surface and 500 hPa and one between 500 hPa and 200 hPa, denoted as the lower and the upper layer respectively. The moisture is contained only in the lower layer, the upper layer is assumed dry. It is further assumed that the relative humidity is constant throughout the lower layer. Moisture that is (vertically) advected into the upper layer is removed by precipitation. In the lower layer precipitation occurs when the relative humidity is larger than 0.8. This is because grid box averaged values are never completely saturated. The amount of precipitation is corrected to account for the heating due to the release of latent heat (latent heat of sublimation in case the surface temperature is below 0°C and latent heat of condensation otherwise). Convective adjustment occurs when the vertical temperature gradient exceeds the dry (moist) adiabatic lapse rate for unsaturated (saturated) conditions.

In a new version of ECBilt (ECBilt2) the radiation schemes are improved. The new radiation parameterizations treat cloud cover explicitly. In addition, the longwave radiation scheme allows for changes in greenhouse gas concentrations and the shortwave radiation scheme can take the direct effect of changes in sulfate aerosol concentrations into account. The parameterization for shortwave radiation (presented in Section 3) and the parameterization for longwave radiation (Schaeffer et al., 1998) are linearizations of fluxes from the radiative transfer model incorporated in the ECHAM4 GCM (Van Dorland, 1999; Morcrette, 1991). In ECBilt2 the representation of clouds has also changed. Cloud cover is either calculated from the simple cloud scheme presented in Section 4 (dynamical clouds) or prescribed (climatological clouds) according to a monthly climatology of the International Satellite Cloud Climatology Project (ISCCP; Rossow et al., 1996) interpolated to the ECBilt resolution. Prescribed clouds are no longer zonally averaged, the longitudinal variations in cloud cover are also taken into account in ECBilt2. The surface albedos for each surface type (land, snow, ocean and sea-ice) are functions of latitude and time of the year. To account for changes in land cover (and land use), surface albedos are linked to different land cover types (Schaeffer et al., 1998) in ECBilt2.

3 Shortwave radiation parameterization

The shortwave radiation parameterization introduced here is basically a linearization of the fluxes of a broad band radiative transfer model. There are two reasons for not using a radiative transfer model directly in an intermediate complexity GCM. Firstly, the vertical resolution of intermediate complexity models is generally too low to give

reliable radiation fluxes. Secondly, by incorporating a sophisticated (and expensive) radiation model the computational efficiency of an intermediate complexity GCM will be seriously affected.

The strategy followed here makes indirect use of the ECHAM4 radiative transfer model, hereafter ECHAM4_RTM (Van Dorland et al., 1999; Morcrette, 1991). The ECHAM4_RTM shortwave fluxes are parameterized in terms of relevant parameters like solar zenith angle, day-fraction (the fraction of the day that the sun is up), surface albedo and cloud fraction. The parameterization involves the linearization of fluxes around a number of reference states. The linearization is performed separately for clear and cloudy skies. The method was first introduced by Chou and Neelin (1996) to derive a linearization of a longwave radiation scheme for the tropics. For the improved longwave radiation scheme for ECBilt2 their method was applied globally to the longwave fluxes of the ECHAM4_RTM (Schaeffer et al., 1998; Schaeffer and Selten, in prep).

A brief description of the ECHAM4_RTM is given next. The radiation scheme is derived from the radiative transfer model of Morcrette (1991) and modified for climate modeling purposes (Van Dorland et al., 1999; Van Dorland et al., in prep.). The model includes the radiative effects of clouds, water vapour, ozone and the well mixed greenhouse gases CO₂, CH₄, N₂O as well as 16 (H)CFC's and HFC's. In addition, 11 aerosol components based on the Global Aerosol Data Set (d'Almeida et al. 1991) are incorporated. The longwave radiative transfer component makes use of 6 spectral intervals, and the shortwave part of the model is divided in 2 spectral intervals; visible and near-infrared.

The solar constant in ECHAM4_RTM was set to 1370 W m⁻². The other variables that served as input to the radiative transfer model and their sources are given below. Profiles of temperature and water vapour are obtained from the 40-year NCEP/NCAR reanalysis (Kalnay et al., 1996). Present day concentrations of CO₂ and the greenhouse gases are adopted from the IPCC (1996). Ozone profiles are based on the ECMWF climatology as in the ECHAM4 model (Roeckner et al., 1996). Surface albedos from the Surface Radiation Budget (SRB) experiment (Darnell et al., 1996) are used. Clouds, finally, are obtained from the International Satellite Cloud Climatology (ISCCP) D2 monthly dataset (Rossow et al., 1996). Cloud parameters of 1990 clouds were used including fractional coverage of low, medium and high clouds, average liquid water path and cloud top pressure. Since the cloud base or thickness can not be determined with satellites, the ISCCP data were combined with the observed cloud base climatology of Poore et al. (1995) as in Rossow and Zhang (1995).

The shortwave radiation parameterization contains a number of steps. First, the shortwave fluxes are linearized around a number of reference states i , determined by reference values of the cosine of the zenith angle $\cos \theta$ and the surface albedo α_s :

$$F_i(\cos \theta, \alpha_s) = \tilde{F}_i + \frac{\partial F_i}{\partial \cos \theta} \Delta \cos \theta + \frac{\partial F_i}{\partial \alpha_s} \Delta \alpha_s \quad i = 1, \dots, 324 \quad (1)$$

in which \tilde{F}_i is the reference flux for the reference state and $\Delta \cos \theta$ and $\Delta \alpha_s$ are respectively the deviations from the reference values of $\cos \theta$ and α_s . In total 324 reference states are distinguished. For each of the 12 calendar months there are 27

regions. Five of these are large mountain regions (Greenland, Rocky Mountains, Himalaya, Andes and Antarctica). The remaining twenty-two regions are obtained by distinguishing land and sea areas in eleven latitude bands (ten 15° bands and one 30° band in the tropics).

The next step is to parameterize the effects of cloud cover variations on the fluxes. The relative simplicity and limited resolution of intermediate complexity models generally limits the number of cloud parameters (and properties) that can be obtained from cloud parameterizations. The simple cloud parameterization that is presented in Section 4) provides e.g. only the total cloud cover. Since we aim to use the simple cloud parameterization in conjunction with the radiation parameterization only the effects of variations in the total cloud cover are taken into account in the radiation parameterization. Based on sensitivity experiments with ECHAM4_RTM it is assumed that for a given vertical distribution of clouds the dependency of the fluxes on the total cloud cover is approximately linear. This means that the flux as function of the total cloud cover can be written as a linear combination of the clear sky and unity overcast fluxes:

$$F_i(c, \mathbf{x}) = (1 - c)F_i^{\text{clr}}(\mathbf{x}) + cF_i^{\text{uoc}}(\mathbf{x}) \quad (2)$$

with c the total cloud cover, \mathbf{x} a two-dimensional vector representing α_s and $\cos \theta$ and, $F_i^{\text{clr}}(\mathbf{x})$ and $F_i^{\text{uoc}}(\mathbf{x})$ the fluxes for the clear sky and unity overcast respectively. The unity overcast fluxes were obtained by scaling the clouds in the ECHAM4_RTM to unity overcast i.e. by dividing the cloud amounts in all cloudy layers in the ECHAM4_RTM (determined by the ISCCP fractions, tops and thicknesses of the low, middle and high clouds) by the total cloud cover. In this way the total cloud amount is maximized while the vertical distribution and the optical properties of the clouds remain unchanged.

Each of the 27 regions consists of several ISCCP grid points. The unity overcast fluxes in the individual ISCCP grid points differ because of differences in the grid box cloud parameters (such as vertical distribution and optical properties). The reference unity overcast flux and the partial derivatives for a particular reference state i are obtained by averaging the fluxes and derivatives of all ISCCP grid points in the corresponding region. As a result climatological variations in vertical cloud distribution and optical thickness (as function of latitude, time of the year and land or sea) are implicitly incorporated in the 324 reference unity overcast fluxes. It is obvious that for the clear sky fluxes no averaging of the ISCCP grid boxes was necessary.

Both for the clear sky and the unity overcast fluxes the $\partial F_i / \partial \cos \theta$'s in Eq. (1) are calculated using finite differences. The variations in the surface albedo (i.e. the deviations from the reference surface albedo) can be substantial in the polar regions and high latitudes as a result of variations in sea ice or land ice coverage. Therefore the derivative $\partial F_i / \partial \alpha_s$ for the clear sky in Eq. (1) is obtained from a linear fit of the response of the clear sky fluxes to possible surface albedo deviations. In contrast to clear sky fluxes it was found that the response of the unity overcast fluxes to deviations from the reference surface albedo is typically non-linear. For best results, the response of unity overcast fluxes to surface albedo variations was fitted to a third order polynomial. For the clear sky and unity overcast fluxes the final form of Eq. (1)

is respectively:

$$F_i^{\text{clr}}(\cos \theta, \alpha_s) = \tilde{F}_i^{\text{clr}} + \frac{\partial F_i^{\text{clr}}}{\partial \cos \theta} \Delta \cos \theta + a_{1,i} \Delta \alpha_s \quad i = 1, \dots, 324 \quad (3)$$

and

$$F_i^{\text{uoc}}(\cos \theta, \alpha_s) = \tilde{F}_i^{\text{uoc}} + \frac{\partial F_i^{\text{uoc}}}{\partial \cos \theta} \Delta \cos \theta + b_{1,i} \Delta \alpha_s + b_{2,i} (\Delta \alpha_s)^2 + b_{3,i} (\Delta \alpha_s)^3 \quad i = 1, \dots, 324 \quad (4)$$

with $a_{1,i}$, $b_{1,i}$, $b_{2,i}$ and $b_{3,i}$ the fitted polynomial coefficients.

The final step in the parameterization is the calculation of the daily average fluxes. In the previous equations $\cos \theta$ is the average cosine of the zenith angle over the time the sun is up. Since the fluxes are zero after sunset, the daily averaged fluxes are obtained by multiplying the fluxes in Eq. (2) with the day-fraction (the fraction of the day the sun is up).

Currently parameterized fluxes are calculated at four vertical levels: top of the atmosphere, 200 hPa, 500 hPa and the surface. The upward and downward fluxes at these levels are calculated separately. Thus for each grid cell 8 fluxes are calculated.

The direct radiative effect of changing sulfate aerosol concentrations is parameterized after Van Dorland (1997). The reflection of solar radiation by sulfate aerosol particles is taken into account as a correction on the upward clear sky fluxes in Eq. (3) using Van Dorland's analytical expression:

$$\Delta F^{\text{clr}\uparrow} = S_0 k (4xy(y-x) - r) \Delta \text{SO}_4 \quad (5)$$

with S_0 the solar constant (1370 W m^{-2}), $k = 0.464 \text{ m}^2 \text{ g}^{-1}$ (assuming a mass scattering coefficient of $8 \text{ m}^2 \text{ g}^{-1}$), $x = (\cos \theta)^{0.5}$, $y = (1 - \alpha_s)^{0.5}$, $r = 0.05$ and ΔSO_4 the change in the column integrated sulfate aerosol concentration in g m^{-2} .

3.1 Performance of the shortwave radiation parameterization

To calculate radiation fluxes with the ECHAM4-RTM a large number of input variables is needed: profiles of temperature and water vapour, concentrations of CO_2 , greenhouse gases and ozone, surface albedos and cloud properties like fractional coverage, vertical distribution and optical thickness. To give an idea of the performance of the ECHAM4-RTM based on those input variables, the ECHAM4-RTM and parameterized fluxes are also compared with the fluxes from 'independent' sources. Fluxes at the top of the atmosphere are compared with the fluxes of the NCEP Reanalysis (Kalnay et al., 1996), the ECHAM4 GCM (Roeckner et al. 1996) and calculations from Kiehl and Trenberth (1997). The surface fluxes are also compared with fluxes from the Surface Radiation Budget (SRB) experiment (Darnell et al., 1996). Table 1 presents the global annual mean fluxes for both the cloudy and clear sky, including the cloud forcing (cloudy sky flux minus clear sky flux). The total shortwave cloud forcing of -50 Wm^{-2} in ECHAM4-RTM agrees well with the results of Kiehl and Trenberth (1997). For the shortwave radiation budget at the surface there is

Table 1: Comparison of global annual mean shortwave radiation fluxes (Wm^{-2}) between NCEP Reanalyses, Surface Radiation Budget (SRB) experiment, Kiehl and Trenberth (1997, denoted as KT97), ECHAM4 GCM, ECHAM4_RTM and the parameterization based on ECHAM4_RTM (LP_RTM).

	NCEP	SRB	KT97	ECHAM4	ECHAM4_RTM	LP_RTM
Top of atmosphere						
Cloudy sky	226	–	235	237	238	241
Clear sky	287	–	285	286	288	288
Cloud forcing	-61	–	-50	-49	-50	-47
Surface						
Cloudy sky	162	161	168	147	155	159
Clear sky	221	214	225	214	218	218
Cloud forcing	-59	-53	-57	-67	-63	-59

currently an uncertainty of 20–25 Wm^{-2} (Kiehl and Trenberth, 1997). According to Kiehl and Trenberth (1997) some of the models used to calculate the annual global mean energy budget, suggest that the net shortwave absorption at the surface would be close to 170 Wm^{-2} while other models and a few observational studies give values around 150 Wm^{-2} . This uncertainty probably results from the uncertainty in the black carbon aerosol (soot) concentrations in the cloudy regions and therefore in the absorption of shortwave radiation by clouds. The ECHAM4_RTM (and ECHAM4 GCM) results are closer to the latter value as a result of a relatively low value of the single scattering albedo (Van Dorland, personal communication).

The parameterization of the shortwave radiation fluxes is validated by comparing monthly mean linearized fluxes with the original fluxes from the radiative-convective model. Figure 1 shows for January and July the differences between the net absorbed shortwave fluxes at the surface in the ECHAM4_RTM and the parameterized fluxes on the $2.5^\circ \times 2.5^\circ$ ISCCP grid. The figure shows that regionally the errors are quite large and in several regions even larger than 50 Wm^{-2} . Much smaller errors can be obtained, however, when the vertical distribution of the clouds and the cloud liquid water path are explicit parameters in the parameterization. In an alternative parameterization that distinguishes low, middle and high clouds and that takes for each cloud type the deviations from the average liquid water path into account, the errors in the shortwave fluxes at the surface are typically smaller than 5 Wm^{-2} (see Fig. 1 right panels). There are a few reasons for not using this alternative parameterization in ECBilt2 so far. Firstly, ECBilt2 can not provide the vertical distributions and optical thicknesses of clouds which therefore have to be prescribed anyway. Secondly, it is more expensive¹. And finally, ECBilt2 operates on a much coarser resolution than the resolution of the

¹Actually the scheme is almost twice as expensive since instead of two calls (one for the clear sky and one for the cloudy sky), four calls are needed (one for the clear sky, one for low, one for middle and one for high clouds).

(gridded) ISCCP cloud climatology on which the validation is based.

4 Cloud cover parameterization

There are roughly two approaches to predict clouds. The first is a diagnostic approach in which clouds are predicted empirically from model variables (see e.g. Slingo 1987). In the second or prognostic approach the cloud water content is an additional prognostic variable. In the prognostic approach the formation and evaporation of cloud and rain drops is explicitly calculated (Sundqvist, 1978). Both approaches make use of a similar formalism to allow for sub-grid scale cloud coverage.

Since cloud water is usually not a variable in intermediate complexity models the cloud scheme introduced here is of the diagnostic type. The cloud formalism allowing for sub-grid scale cloud formation developed by Sundqvist (1978) is followed. In this formalism the grid box mean specific humidity q_v is written as

$$q_v = cq_{sat}(T, p) + (1 - c)q_e, \quad (6)$$

where c denotes the fractional horizontal area of a grid box covered with clouds. The fraction $1 - c$ thus refers to the cloud-free part. q_e is the specific humidity in the cloud-free fraction. It is assumed that the in-cloud specific humidity is equal to the saturation specific humidity q_{sat} . Equation (6) can be rewritten to give the cloud fraction

$$c = \frac{q_v - q_e}{q_{sat} - q_e} \quad (7)$$

where the specific humidity in the cloud-free part q_e remains to be determined. In the original formulation of Sundqvist (1978) q_e is simply set equal to a threshold specific humidity q_0 . In a later formulation (Sundqvist, 1988) q_e is a function of the cloud fraction

$$q_e = cq_{sat}(T, p) + (1 - c)q_0. \quad (8)$$

A mathematical advantage of Eq. (8) is that the cloud fraction c can be differentiated in the point $q_v = q_0$. The expression for q_e given in Eq. (8) is e.g. used in ECHAM4. Here $q_e = q_0$ is used as in the ECHAM3 model. The cloud fraction c can then be expressed in terms of relative humidity by dividing numerator and denominator of Eq. (7) by q_{sat}

$$c = \frac{r - r_0}{1 - r_0} \quad (9)$$

where r is the relative humidity and r_0 is the threshold relative humidity. The threshold r_0 is often a function of height and stability. In ECBilt only one layer with moisture exist and therefore only one cloud layer can be determined with the cloud scheme described. A tuned value of 0.5 for r_0 gave a global annual mean cloud cover close the observed value. No distinction is made between different stability classes. Instead an alternative expression for the cloud cover is used that distinguishes upward and downward vertical motion and that is similar to the expression for stratocumulus clouds in ECHAM4 (Roeckner et al., 1996)

$$c = \frac{r/f - r_0}{1 - r_0}. \quad (10)$$

For subsiding air ($\omega_{650} > 0$) the factor f is set to 1.0 and for ascending air f is set to 0.95 ($-0.04 < \omega_{650} < 0$) and 0.9 ($\omega_{650} < -0.04$). To enhance the simulation of marine stratocumulus clouds associated with a strong subsidence inversion f is set to 0.7 if $\omega_{650} > 0.03$ at sea points. The cloud fraction is set to zero when $r/f < r_0$ and to unity when $r/f > 1$.

4.1 Performance of the cloud parameterization in ECBilt

To investigate the performance of this cloud scheme in ECBilt, ECBilt2 is coupled to a 80 m slab ocean and integrated for 100 years. The simulated total cloud cover is compared with 'observed' ISCCP total cloud cover. First the average cloud cover is discussed and then the cloud cover variability.

4.1.1 Average cloud cover

Figure 2 presents simulated and observed ISCCP cloud cover for DJF (December–February) and JJA (June–August). The global mean values for the NH winter are respectively 0.58 and 0.60. Over land the simulated cloud cover is in general lower than over the ocean. Compared with the observations this land-sea contrast is too pronounced. The storm tracks in the northern and southern hemisphere are captured although cloud coverage is slightly smaller than observed. Local minima such as those over Greenland, northern Africa, Australia and Antarctica are also simulated. The observed minimum over south east Asia is shifted to the north in the simulation but the minima over the (sub)tropical oceans are not well simulated. The simulated minimum over a large part of the U.S. is much too pronounced compared to the observations. The differences between simulations and observations for JJA are similar in nature as for DJF although the differences can be more pronounced locally.

4.1.2 Cloud cover variability

Interannual variability

Simulated and observed inter-monthly standard deviations of cloud cover for DJF and JJA are presented in Figure 3. Both in the simulations and the observations the inter-monthly standard deviation of cloud cover is relatively small; roughly between 0.02 and 0.10. The storm tracks are characterized by a small inter-monthly variability which is also found in the simulated cloud cover. In the simulations the variability over land is generally larger than over the oceans. Compared with the observations this land-sea contrast is overestimated. In the observations the interannual variability is relatively large over the (sub)tropical oceans, in particular during DJF, but the simulated variability is relatively small in that area.

Daily variability

Figure 4 shows simulated daily standard deviation of cloud cover for DJF and JJA and observed (ISCCP) daily standard deviation for January and July of the year

1988. Daily standard deviation is defined here as the variations of the daily values with respect to the individual monthly means. This standard deviation is sometimes referred to as within-month standard deviation. The daily standard deviations for DJF and JJA are obtained by averaging the daily standard deviations over the calendar months of a seasons. Note that the daily standard deviations are on average about three times as large as the monthly standard deviations. The daily standard deviations of the simulated and observed cloud cover are similar in magnitude but their patterns differ considerably. In the simulation the patterns of daily cloud cover variability have a much larger scale structure than in the observations. Further, the simulated patterns depend much more on the seasons than the observed ones. For the observations there will be a relatively large sampling uncertainty due to the short record length (one year only).

5 The ECBilt2 climatology: dynamical versus climatological clouds

This section is devoted to a comparison of the climatology of the ECBilt2 model with prescribed cloud cover (referred to as 'climatological cloud simulation') and the ECBilt2 model in which the the cloud cover is calculated with the simple cloud scheme presented in the previous section (referred to as 'dynamical cloud simulation'). In the climatological cloud simulation the seasonal cycle of the cloud cover is represented by using a monthly cloud cover climatology. In the dynamical cloud simulation there are, in contrast to the climatological cloud simulation, daily and interannual variations in cloud cover which may influence the model mean state and its variability through induced variations in the radiation balance.

To minimize sampling differences both simulations were performed for a period of 100 years. As in the previous section ECBilt2 was coupled to a slab ocean. The impact of dynamical cloud cover on the surface temperature, geopotential height and diabatic heating is discussed. The changes in mean conditions as well as the changes in variability are considered.

5.1 Surface temperature

Differences in surface temperature² between the simulation with dynamical clouds and the simulation with prescribed climatological clouds for DJF and JJA are given in Figure 5. The surface temperature is on average lower in the simulation with dynamical clouds than in the simulation with climatological clouds. Over the oceans the temperature differences are typically within 1 °C. Over land larger differences up to 5 °C are found. Temperatures over land in the dynamical cloud simulation are mostly smaller in DJF while in JJA also a few regions with considerably larger temperatures are present in this simulation. Almost everywhere over land and sea and for both presented seasons these differences are statistically significant at the 5%-level (*t*-test).

²The surface temperature represents the land surface temperature over land and the sea surface temperature over the oceans.

Figure 6 presents interannual and daily surface temperature standard deviation ratios of the simulation with dynamical clouds and the simulation with climatological clouds for DJF and JJA. The ratios of the interannual standard deviations (top panels) are mostly larger than 1 in particular over the continents. Large continental areas experience interannual standard deviations that are 20–50% larger in the simulation with dynamical clouds than with climatological clouds. Daily standard deviations (lower panels) are also enhanced by 10 to 20%. In JJA over a large parts of Europe, Asia and Antarctica increases of 20–50% occur. The largest reductions of interannual and daily standard deviations are found in JJA along the Antarctic sea-ice edge. This reduction is associated with larger SSTs in this area in the dynamical cloud simulation which in turn affects sea-ice formation.

5.2 Geopotential height

In this subsection differences in geopotential height are presented to indicate the differences in the atmospheric circulation between the dynamical cloud simulation and the simulation with prescribed climatological clouds. Geopotential height differences at three levels - 200, 500 and 800 hPa - are presented in Figure 7. Two positive height anomalies centred over Europe and the eastern Pacific at 60° N are found at 800 and 500 hPa. At 200 hPa these anomalies are connected and form a long zonal band. The magnitude of the anomalies increases with height indicating that they are associated with positive temperature anomalies. As a result a weaker westerly circulation is expected. A reduced strength of the westerlies also implies a weakening of the storm activity. A simple measure of the storm activity is the daily standard deviation of the geopotential height. Weakening of the westerlies should therefore be visible as a reduction of the geopotential height daily standard deviation. The variability associated with the storm activity is most pronounced at 200 hPa. The difference in the daily standard deviation of the 200 hPa geopotential height in DJF between the two simulations is presented in Figure 8. To give an idea of the location and strength of the largest storm activity the lower panel of the figure presents the daily standard deviation of the 200 hPa height in the climatological cloud simulation in DJF. The figure shows that indeed a considerable reduction in variability is found along the North Atlantic storm track. As a consequence this storm track extends less deep into Western Europe.

5.3 Diabatic heating

The geopotential height anomalies that we saw earlier must be related to anomalous diabatic heating. In ECBilt2 the diabatic heating takes place in two layers. The first layer between 1000 and 500 hPa and the second layer between 500 and 200 hPa. Figure 9 presents for the two layers the difference in diabatic heating in DJF between the simulation with dynamical clouds and the simulation with climatological clouds. In the lowest layer two positive heating anomalies can be identified in the northern extra-tropics which lie slightly upstream of the geopotential height anomalies presented in Figure 7. These heating anomalies are related to changes in the sensible

and latent heat fluxes (not shown). In addition to the $Q_{500-1000}$ heating anomalies there is also a positive heating anomaly in $Q_{200-500}$ over the U.S. Together with the $Q_{500-1000}$ anomalies this anomaly gives rise to the anomalous positive temperatures and geopotential heights (Figure 7). The $Q_{200-500}$ anomaly over the U.S. appears to be related to the underestimation of the cloud cover in this region. For low clouds, which is the major cloud type in this region, the longwave cloud forcing at the surface is larger than at the top of the atmosphere as a result of the large black body radiation from the low (i.e. warm) cloud base. This means that the radiative cooling of the atmosphere is larger when clouds are present, so less clouds over the U.S. give rise to less atmospheric cooling and thus results in an effective warming of the atmosphere as reflected in $Q_{200-500}$.

5.4 Summary and discussion of the differences

Changing from a climatological clouds scheme to a dynamical cloud scheme in ECBilt not only leads to an enhanced variability of the surface temperature but also to a significant different mean climate. These differences in mean climate are due to systematic differences between average simulated cloud cover and the observed cloud cover climatology. The differences in the surface temperature climatology are almost everywhere statistically significant.

Cloud cover induced heating anomalies lead to a weakening of the westerly circulation in the NH winter with an associated weakening of the storm activity, in particular in the North Atlantic storm track. The changes in the (modeled) natural variability are thus not only due to the introduction of cloud cover variability but also to the changes in the mean cloud cover climatology. In order to distinguish between changes in variability resulting from changes in the simulated mean cloud climatology and those resulting from the introduction of cloud cover variability, a second dynamical cloud simulation was performed. In this so called *anomaly cloud simulation* daily cloud cover anomalies with respect to the simulated (dynamical) monthly mean cloud cover climatology were added to the observed monthly mean cloud cover climatology³. Such an approach, in which the simulated cloud cover climatology is almost identical to the observed cloud cover climatology but in which the cloud cover variability of the dynamical cloud cover scheme is preserved, is typical for flux-corrections. In the next section the results of the anomaly cloud simulation are compared with the climatological cloud simulation in a similar way as for the dynamical cloud simulation.

6 The ECBilt2 climatology: anomaly versus climatological clouds

The anomaly cloud simulation is also integrated for a period of 100 years. The differences in average cloud cover between the two schemes are generally within 0.02 (not

³In addition the cloud cover is bounded between 0 and 1; i.e. if the cloud cover becomes smaller than zero it is set to zero and if it becomes larger than one it is set to one.

shown). Equivalently, the differences in average longwave and shortwave fluxes are generally within a few Wm^{-2} .

In addition to the differences in surface temperature, geopotential height and diabatic heating also the differences in the precipitation climatology are presented.

6.1 Surface temperature

Surface temperature differences both in DJF and JJA are mostly within 0.3°C . Differences of up to 1.5°C are found along the Antarctic sea-ice edge in JJA. Although the temperature differences are about three times as small as in the case of dynamical versus climatological clouds, there is still quite a large number of sea grid points for which these differences are statistically significant based on a t -test at the 5% level. (not shown).

Figure 10 shows the interannual and daily surface temperature standard deviation ratios of the anomaly cloud simulation and the climatological cloud simulation for DJF and JJA. In particular in the NH summer large continental areas experience increases of 20–50% in the interannual standard deviations. In the anomaly cloud simulation the increases in the interannual standard deviation are on average somewhat smaller than those in the dynamical cloud simulation (Figure 6, upper panels). In JJA the global average increases are respectively 11% and 15%, in DJF the increases are about 7% for both simulations.

The changes in the daily standard deviations (lower panels) have similar characteristics as the changes in the interannual standard deviations. On average the increases in the anomaly cloud simulation are somewhat smaller than the increases in the dynamical cloud simulation (Figure 6, lower panels). The global average increase for DJF en JJA are respectively 5% and 7% in the anomaly cloud simulation, while in the dynamical cloud simulation these increases are 7% and 10%.

Both for the interannual and the daily standard deviations, some of the regional changes (increases or decreases) are robust while others are not. For a number of regions there also seems to be a strong correlation between changes in daily and interannual variability.

6.2 Geopotential height

Figure 11 presents the differences in geopotential height (anomaly minus climatological clouds) at 200, 500 and 800 hPa for DJF. Comparison with Figure 7 (dynamical minus climatological clouds) shows that the geopotential height anomalies are now about 3-5 times as small. None of these anomalies is statistically significant (t -test at the 5% level) apart from a tropical band in the 200 hPa difference in which the t -values are slightly larger than 2 (not shown).

The difference in daily standard deviation of the geopotential height at 200 hPa in DJF between both simulations is given in Figure 12. The smaller anomalies in the geopotential height lead to smaller changes in storm track variability. The changes between the anomaly and climatological cloud simulations correspond to small shifts

(displacements) of storm track variability instead of systematic decreases of storm track variability as in the dynamical cloud simulation.

6.3 Diabatic heating

In the anomaly cloud simulation there are no large diabatic heating anomalies (not shown). This is not surprising since there are neither large geopotential height anomalies nor large cloud cover anomalies.

In winter (DJF) there are a few (sub)tropical regions for which considerable increases (up to 100%) in daily and interannual standard deviations of $Q_{200-500}$ are found. Figure 13 shows that the two most pronounced regions lie east of South-America and east of South-Africa. For the same regions also increases in daily and interannual standard deviations of $Q_{500-1000}$ are found although they are somewhat less pronounced (not shown). Similar increases are also found when comparing the dynamical and climatological cloud simulations (not shown). The diabatic heating involves four terms: absorption of shortwave radiation, longwave radiative cooling, release of latent heat and a sensible heat flux. The introduction of cloud cover variability considerably enhances the variability of the individual components, in particular for the absorption of solar radiation and the longwave cooling. On the diabatic heating the effects of clouds are however partly compensated by the different terms. Depending on the type of clouds the longwave and shortwave radiative forcings may e.g. largely cancel. Also the sensible heat flux tends to damp the effects of clouds in the diabatic heating. The increase in the variability for the diabatic heating is thus on average smaller than for the shortwave absorption and the longwave cooling alone. In the regions where the increase in the diabatic heating variability is most pronounced the compensation of the different terms is apparently least effective.

6.4 Precipitation

Both for winter (JJA) and summer (DJF) the differences in mean precipitation⁴ amounts between the anomaly cloud simulation and the climatological cloud simulation are not significant (not shown).

Figure 14 shows the interannual and daily precipitation standard deviation ratios of the anomaly cloud simulation and the climatological cloud simulation for DJF and JJA. There are areas with reduced as well as enhanced precipitation variability. Reduced variability is mainly found in the tropics while enhanced variability is typically found in the sub-tropics and mid-latitudes. Increases between 5 and 20% are found for the monthly precipitation standard deviation around 30° N in summer, including large parts of the North-American and European continents.

6.5 Summary and discussion of the differences

The mean climate of the anomaly cloud simulation is very similar to that of the climatological cloud simulation compared with the dynamical cloud simulation. Only

⁴Large scale + convective precipitation

a few of the analyzed differences are statistically significant. Apart from a similar mean climate there are systematic increases in the daily and interannual variability which are related to the incorporation of cloud cover variability. Most pronounced are the increases in the surface temperature and precipitation variability in summer over northern hemisphere mid-latitude land areas. In the tropics a few regions with reduced precipitation variability were found.

By comparing the changes in variability in the anomaly cloud simulation with those in the dynamical cloud simulation it is possible to distinguish variability changes due to cloud cover variability from variability changes due to differences in model climatology. The anomaly cloud simulation confirms that e.g. the considerable reduction of daily geopotential height variability in the North Atlantic storm track in winter and the enhanced monthly variability of the surface temperature over central North America and central Asia in winter in the dynamical cloud simulation are due to differences in the mean climate rather than the incorporation of cloud cover variability.

7 Discussion and conclusions

Since systematic errors in the simulated cloud cover in the dynamical cloud simulation lead to systematic differences in the mean climate and the variability of the model it is recommended to incorporate cloud cover variability in the same way as in the anomaly cloud simulation i.e. by using only the simulated cloud cover anomalies (from the dynamical cloud scheme presented in Section 4) and adding those to the observed mean cloud cover climatology. In integrations of ECBilt2 coupled to a slab ocean the incorporation of cloud cover variability gave rise to enhanced daily and interannual surface temperature and precipitation variability, in particular in summer (JJA). In this study the effects were only analyzed for a limited number of variables. For a more complete picture more variables should be analyzed.

The question if enhanced variability on daily to interannual time scales also influences the decadal variability is not resolved. To answer this question much longer anomaly cloud simulations with ECBilt2 coupled to a real ocean model have to be performed. Such coupled versions of ECBilt are already available. The ocean model of Lenderink and Haarsma (1994) was used in Haarsma et al. (1996; 1997) and Opsteegh et al. (1998) while Goose et al. (2001) used the more sophisticated CLIO model which also has a dynamic instead of a thermodynamic sea-ice model.

Although it is possible to incorporate cloud cover variability in the model without changing the mean climate of the model too much, and although the simulated cloud cover variability has on average the right magnitude, one should keep in mind that the spatial patterns of the daily and interannual cloud cover variability are not perfect when compared to the observed variability patterns. This will probably affect the realism of the (enhanced) variability patterns in simulations with dynamical cloud cover but this does not necessarily mean that such simulations are *unrealistic* or that the model is not suitable to study the effects of cloud variability on model variability in general. Before any conclusions can be drawn the (enhanced) variability patterns in ECBilt2 first have to be compared with variability patterns from the observations.

In this study the longwave and shortwave parameterizations based on one cloud type (i.e. total cloud cover) were used. Alternative parameterizations were developed based on three cloud types (low, middle and high clouds). Although the parameterizations based on three cloud types gave much smaller errors in the validation they were not used for practical reasons. Still, it would be interesting to study how these alternative parameterizations would perform in ECBilt2. The simple cloud scheme, which gives only the total cloud cover, can be combined with the radiation parameterizations based on three cloud types when the vertical distribution of clouds is prescribed. A spatially and temporally varying climatology of the distribution between low, middle and high clouds can be derived from the ISCCP climatology. Although the total cloud cover variability will not change (much) in such an experiment the radiative effects can be quite different since the radiative effects depend strongly on the cloud type.

Finally, the new shortwave radiation parameterization is an improvement not only because of the possibility to include cloud cover variability. In simulations with prescribed cloud cover the radiative effects of clouds are now also meridionally varying. With the new shortwave radiation parameterization it is further possible to account for the direct effect of changes in the sulfate aerosol concentrations which makes the shortwave scheme suitable for anthropogenic climate change simulations.

Acknowledgements

The authors are very grateful for the collaboration and fruitful discussions with R.J. Haarsma, M. Schaeffer and F.M. Selten during the project. C.-T. Chen is acknowledged for providing the daily standard deviations of the ISCCP total cloud cover.

References

- d'Almeida, G.A., Koepke, P., Shettle, E.P. 1991. *Atmospheric Aerosols Global Climatology and Radiative Characteristics*, A. Deepack, Hampton, Va., USA.
- Chen, C.-T. and Roeckner, E. 1997. Cloud simulations with the Max-Planck-Institute for Meteorology general circulation model ECHAM4 and comparison with observations. Max-Planck-Institute for Meteorology, Report No. 193, Hamburg, 49 pp. *J. Geophys. Res.*, **102**, 17, 9335-9350.
- Chou, C. and Neelin, J.D., 1996. Linearization of a longwave radiation scheme for intermediate tropical atmospheric models. *J. Geophys. Res.*, **101**, D10, 15,129-15,145.
- Darnell, W.L., Staylor, W.F., Ritchey, N.A., Gupta, S.K. and Wilber, A.C., 1996. Surface Radiation Budget: A Long-term Global Dataset of Shortwave and Longwave Fluxes. http://www.agu.org/eos_elec/95206e.html
- Goosse, H., Selten, F.M., Haarsma, R.J. and Opsteegh, J.D., 2001. Decadal variability in high northern latitudes as simulated by an intermediate-complexity climate model. *Ann. Glaciol.*, **33** (in press).
- Haarsma, R.J., Selten, F.M., Opsteegh, J.D., Lenderink, G. and Liu, Q. 1996. EC-BILT: A coupled Atmosphere Ocean Sea-ice model for climate predictability studies. KNMI Technical Report TR-195. Royal Netherlands Meteorological Institute (KNMI), De Bilt, The Netherlands.
- Haarsma, R.J., Selten, F.M., Opsteegh, J.D. and Kattenberg, A. 1997. North-Atlantic decadal climate variability in a coupled atmosphere/ocean/sea-ice model of moderate complexity. KNMI Report. Royal Netherlands Meteorological Institute (KNMI), De Bilt, The Netherlands.
- Held, I.M. and Suarez, M.J., 1978. A two level primitive equation atmosphere model designed for climate sensitivity experiments. *J. Atmos. Sci.*, **35**, 206-229.
- Holtzlag, A.A.M. and van Ulden, A.P. 1983. A simple scheme for daytime estimates of the surface fluxes from routine weather data. *J. Appl. Meteor.*, **22**, 517-529.
- IPCC (Intergovernmental Panel on Climate Change), 1996. *Climate Change 1995, The Science of Climate Change*, Houghton, J.T., Meira Filho, L.G., Callander, B.A., Harris, N., Kattenberg, A. and Maskell, K. (eds.) 572 pp., Cambridge University Press, Cambridge, UK.
- Kalnay, E., Kanamitsu, M., Kistler, R., Collins, W., Deaven, D., Gandin, L., Iredell, M., Saha, S., White, G. Woollen, J., Zhu, Y., Chelliah, M., Ebisuzaki, W., Higgins, W., Janowial, J., Mo, K.C., Ropelewski, C., Wang, J., Leetmaa, A., Reynolds, R. Jenne, R. and Joseph, D. 1996. The NCEP/NCAR 40-Year Reanalysis Project. *Bull. Amer. Meteor. Soc.*, **77**, 437-471.
- Kiehl, J.T. and Trenberth, K.E. 1997. Earth's annual global mean energy budget. *Bull. Amer. Meteor. Soc.*, **78**, 197-208.
- Lenderink, G. and Haarsma, R.J. 1994. Variability and multiple equilibria of the thermohaline circulation associated with deep water formation. *J. Phys. Oceanogr.*, **24**, 1480-1493.
- Marshall, J. and Molteni, F. 1993. Towards a dynamic understanding of planetary-scale flow regimes. *J. Atmos. Sci.*, **50**, 1792-1818.

- Morcrette, J.-J., 1991. Radiation and cloud radiative properties in the European Centre for Medium Range Weather Forecasting system, *J. Geophys. Res.*, **96**, 9121-9132.
- Opsteegh, J.D., Haarsma, R.J., Selten, F.M., Kattenberg, A., 1998. ECBILT: a dynamic alternative to mixed boundary conditions in ocean models. *Tellus*, **50A**, 348-367.
- Poor, K.D., Wang, J. and Rossow, W.B., 1995. Cloud layer thicknesses from a combination of surface and upper-air observations. *J. Climate*, **8**, 550-568
- Roeckner, E., Arpe, K., Bengtsson, L., Christoph, M., Claussen, M., Dümenil, Esch, M., Giorgetta, M., Schlese, U. and Schulweida, U., 1996. The atmospheric general circulation model ECHAM-4: model description and simulation of present-day climate. Report 218, Max-Planck Institute for Meteorology, Hamburg, Germany.
- Rossow, W.B., Zhang, Y.-C., 1995. Calculation of surface and top of atmosphere radiative fluxes from physical quantities based on ISCCP data sets. 2. Validation and first results. *J. Geophys. Res.*, **100**, D1, 1167-1197.
- Rossow, W.B., Walker, A.W., Beuschel, D.E. and Roiter M.D., 1996. International Satellite Cloud Climatology project (ISCCP): Documentation of New Cloud Datasets. WMO/TD-No. 737, World Meteorological Organization, 115 pp.
- Schaeffer, M., Selten, F. and Van Dorland, R. 1998. Linking IMAGE and ECBILT. National Research institute for Public Health and the Environment (RIVM), Bilthoven, The Netherlands.
- Schaeffer, M., Selten, F.M., in prep. Implications of a sudden transition for uncertainties in climate change projections. To be submitted to *Climate Dynamics*.
- Semtner, A.J. 1976. A model for the thermodynamic growth of sea-ice in numerical investigations of climate. *J. Phys. Oceanogr.*, **6**, 379-389.
- Slingo, J.M. 1987. The development and verification of a cloud prediction scheme for the ECMWF model. *Q. J. R. Meteorol. Soc.*, **113**, 899-927.
- Sundqvist, H. 1978. A parameterization scheme for nonconvective condensation including prediction of cloud water content. *Q. J. R. Meteorol. Soc.*, **104**, 677-690.
- Van Dorland, R., Dentener, F.J. and Lelieveld, J., 1997. Radiative forcing due to tropospheric ozone and sulfate aerosols. *J. Geophys. Res.*, **102**, 28,079-28,100.
- Van Dorland, R., Stammes, P., Holtslag, A.A.M. and Kohsiek, W., 1999. A longwave radiative transfer scheme for climate modelling and its evaluation with surface observations at Cabauw. KNMI Preprints 99-09, Royal Netherlands Meteorological Institute (KNMI), De Bilt, The Netherlands
- Van Dorland, R., Stammes, P., Holtslag, A.A.M. and Kohsiek, W., in prep. A longwave radiative transfer scheme for climate modelling and its evaluation with surface observations at Cabauw.

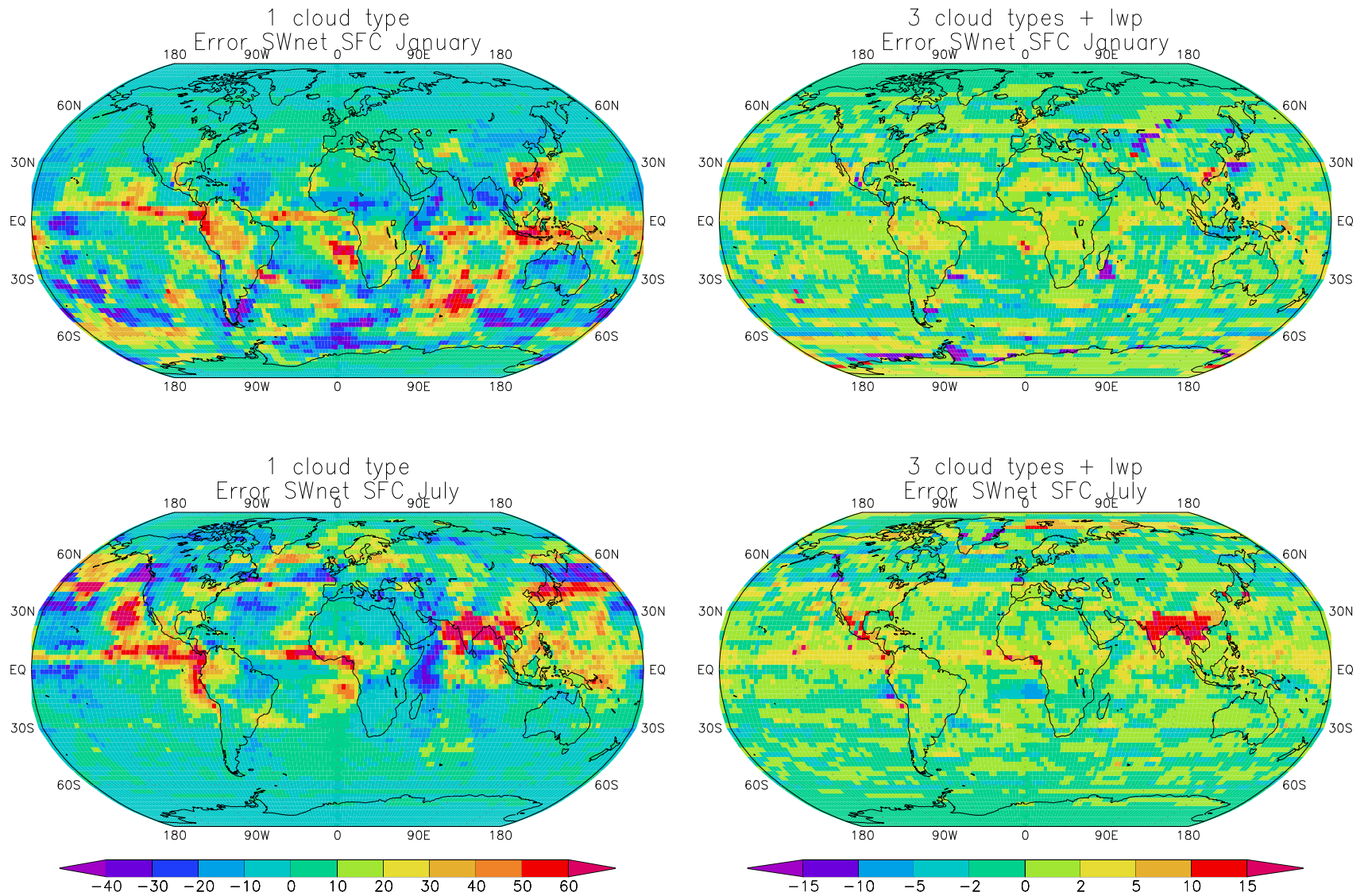


Figure 1: Difference between ECHAM4-RTM net absorbed shortwave fluxes at the surface and the parameterized fluxes at the surface for January and July. Left panels: parameterization with one cloud type; right panels: parameterization with 3 cloud types and explicit function on cloud liquid water path (lwp). Units are Wm^{-2} .

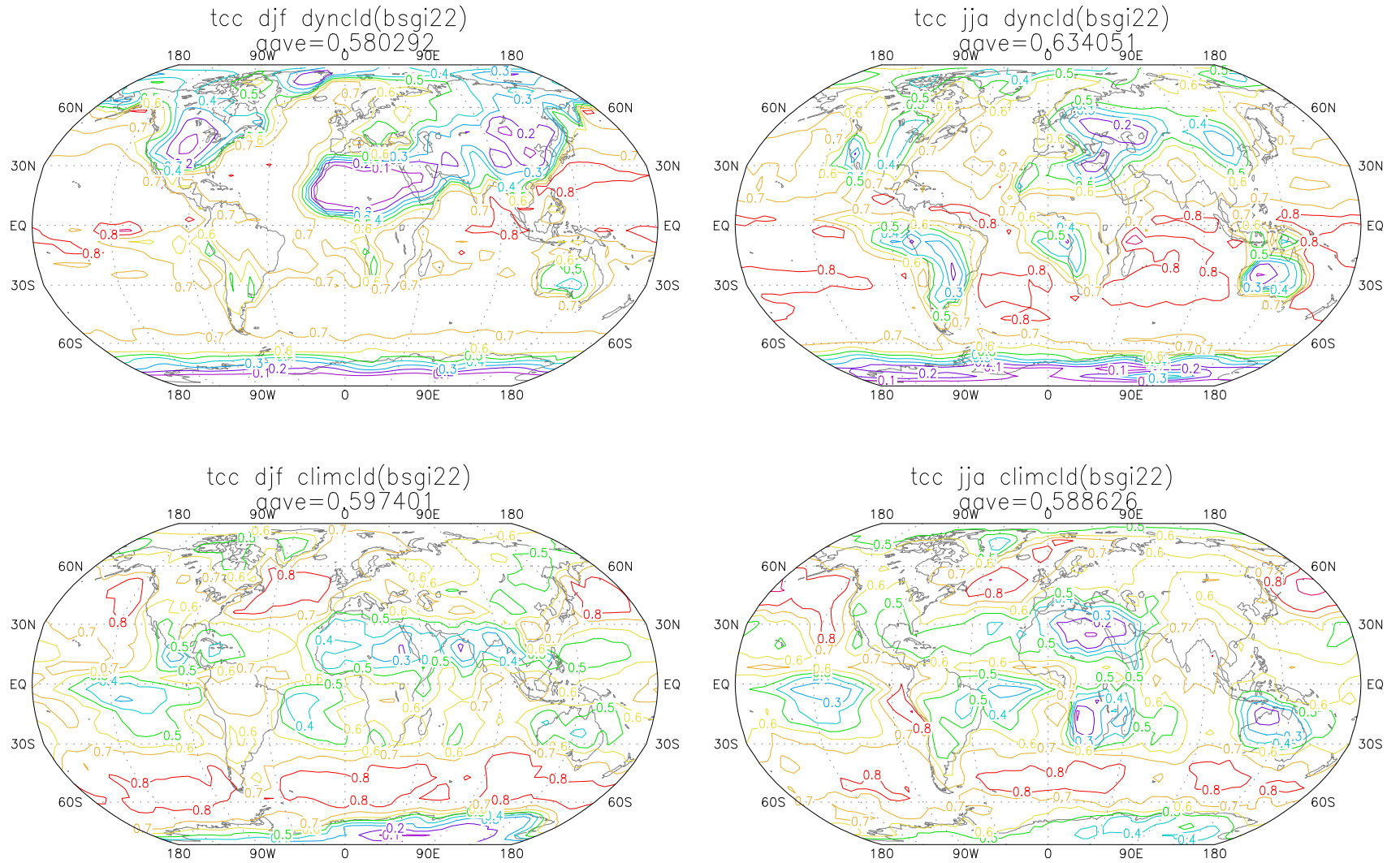


Figure 2: Simulated (upper panels) and observed ISCCP total cloud cover for DJF (December–February) and JJA (June–August).

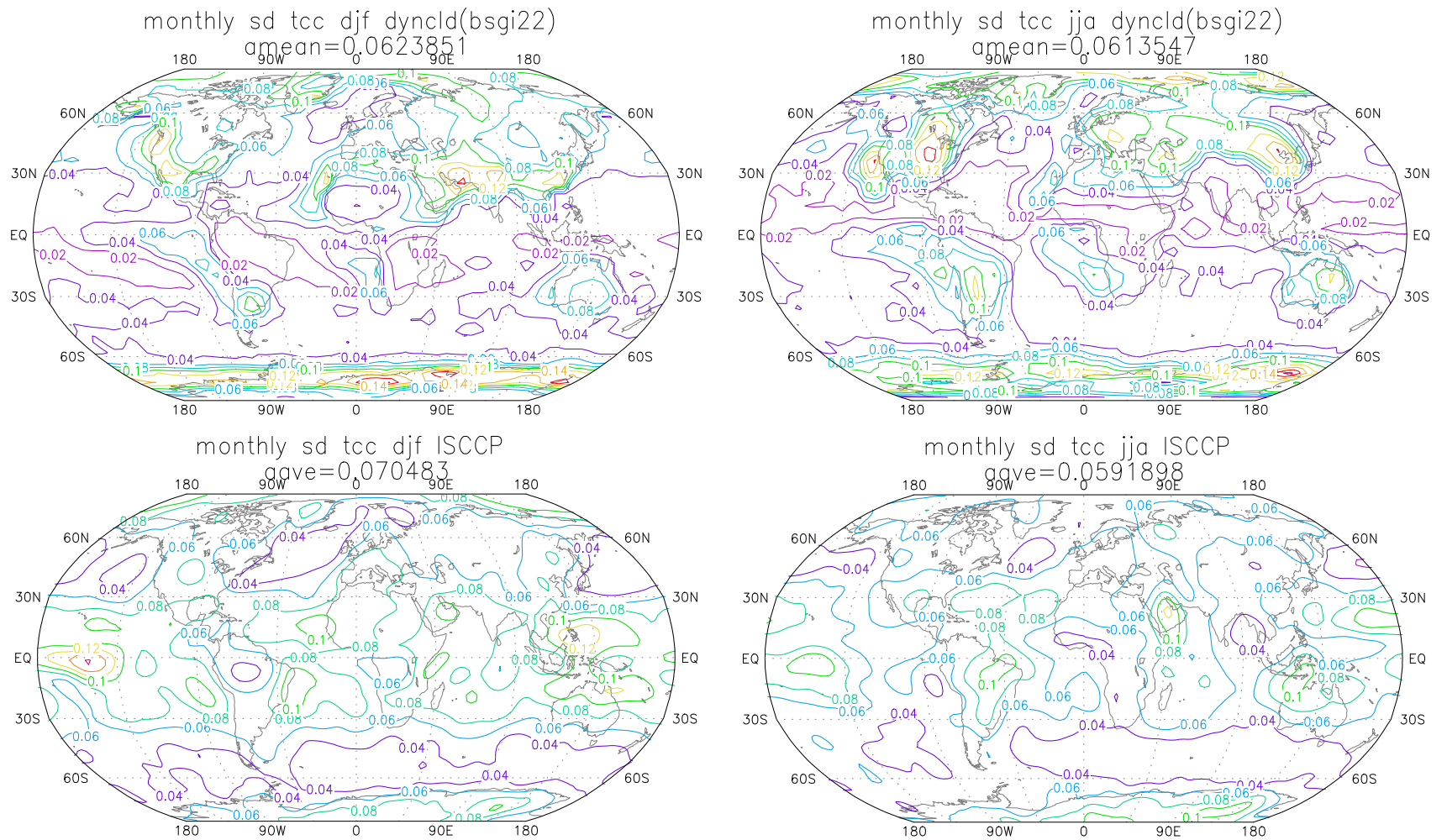


Figure 3: Simulated (upper panels) and ISCCP inter-monthly standard deviation of cloud cover for DJF and JJA. ISCCP data are smoothed for presentation

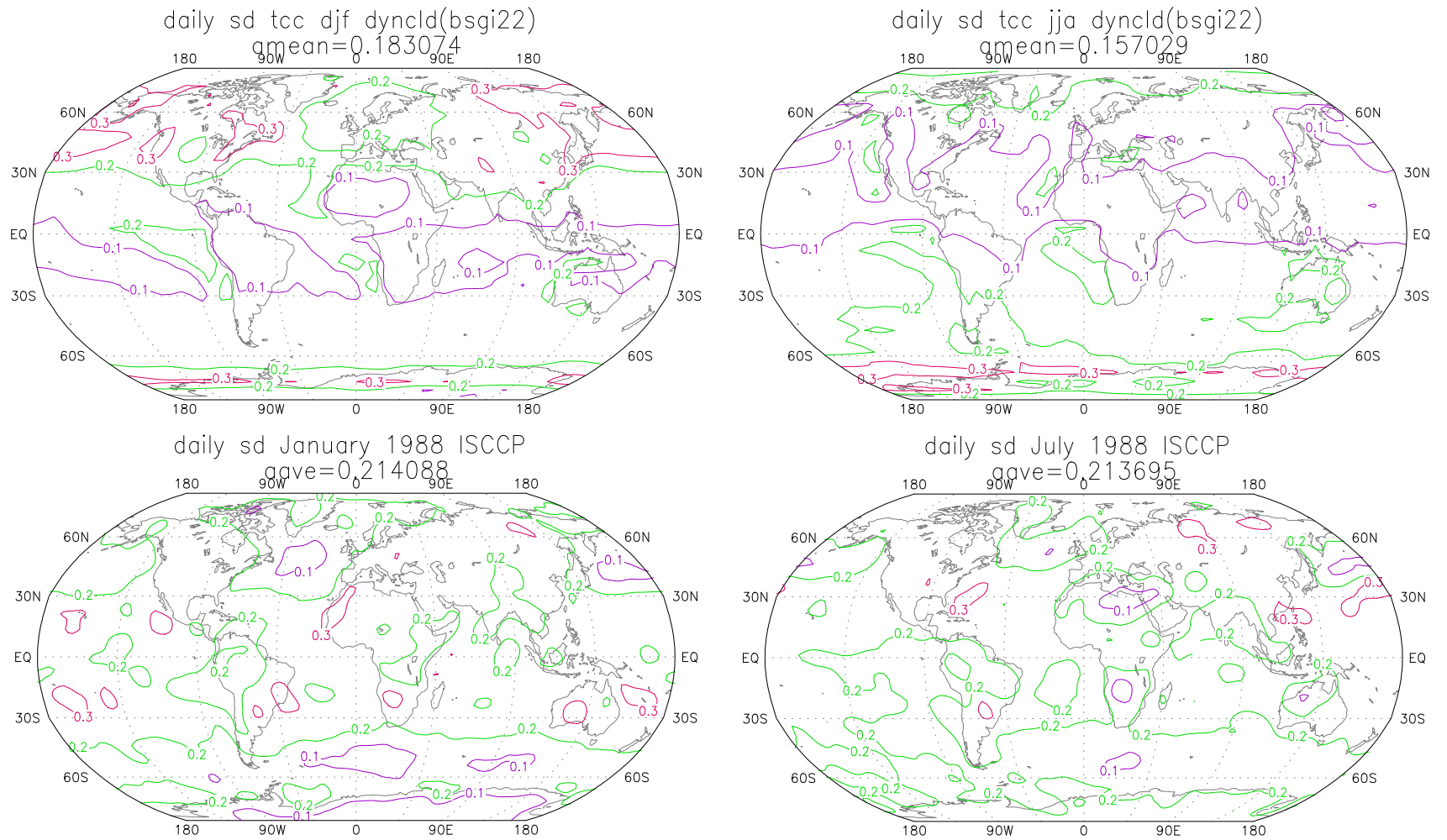


Figure 4: Simulated daily standard deviation of cloud cover for DJF and JJA (upper panels), and ISCCP daily standard deviations for January 1988 and July 1988. ISCCP data are obtained from Chen and Roeckner (1997) and smoothed for presentation.

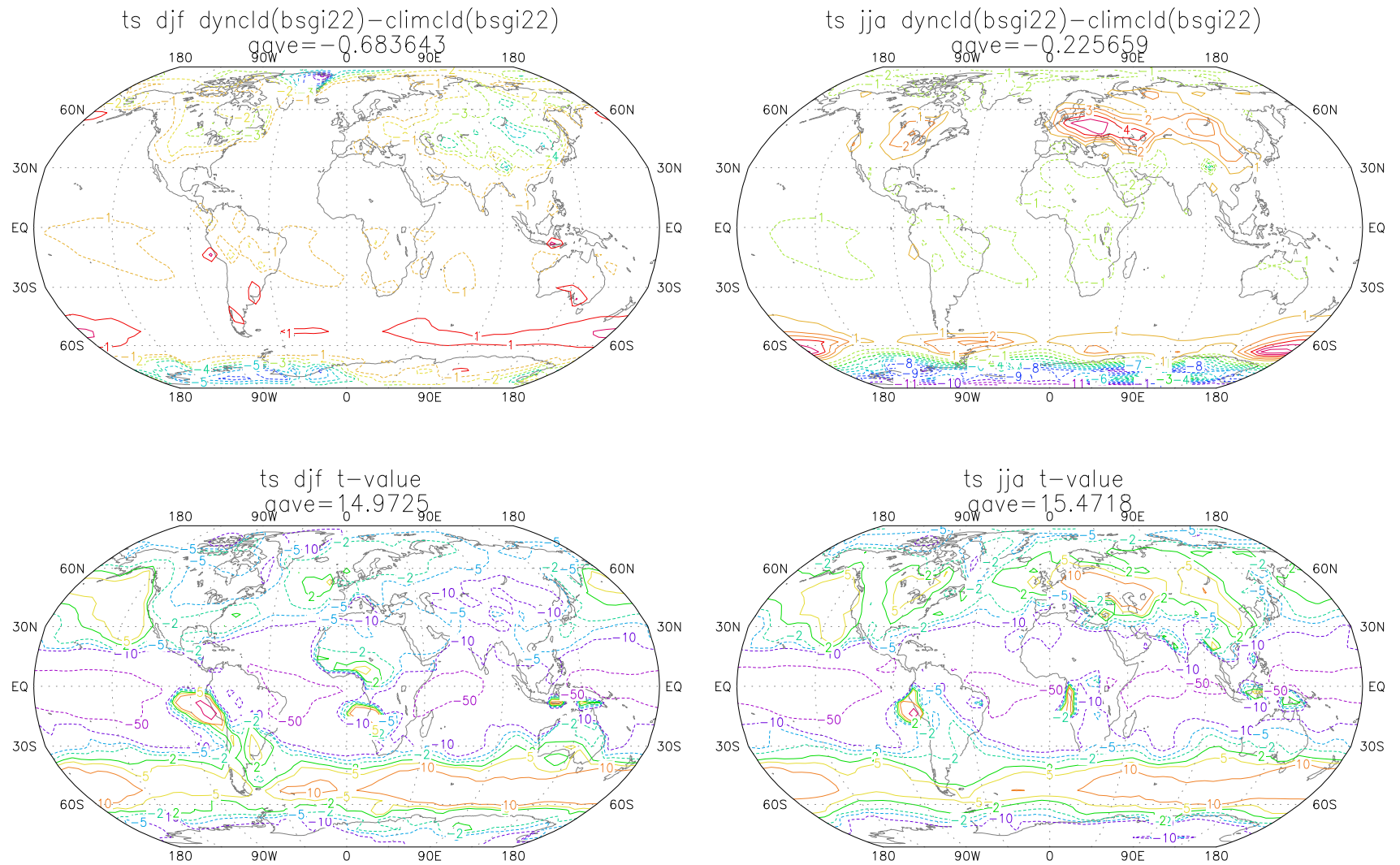


Figure 5: Difference in surface temperature ($^{\circ}\text{C}$) between the simulation with dynamical clouds and the simulation with prescribed climatological clouds for DJF and JJA. The lower panels give the corresponding t -values of the differences. t -values larger than 2 or smaller than -2 roughly denote statistically significant differences at the 5%-level (t -test).

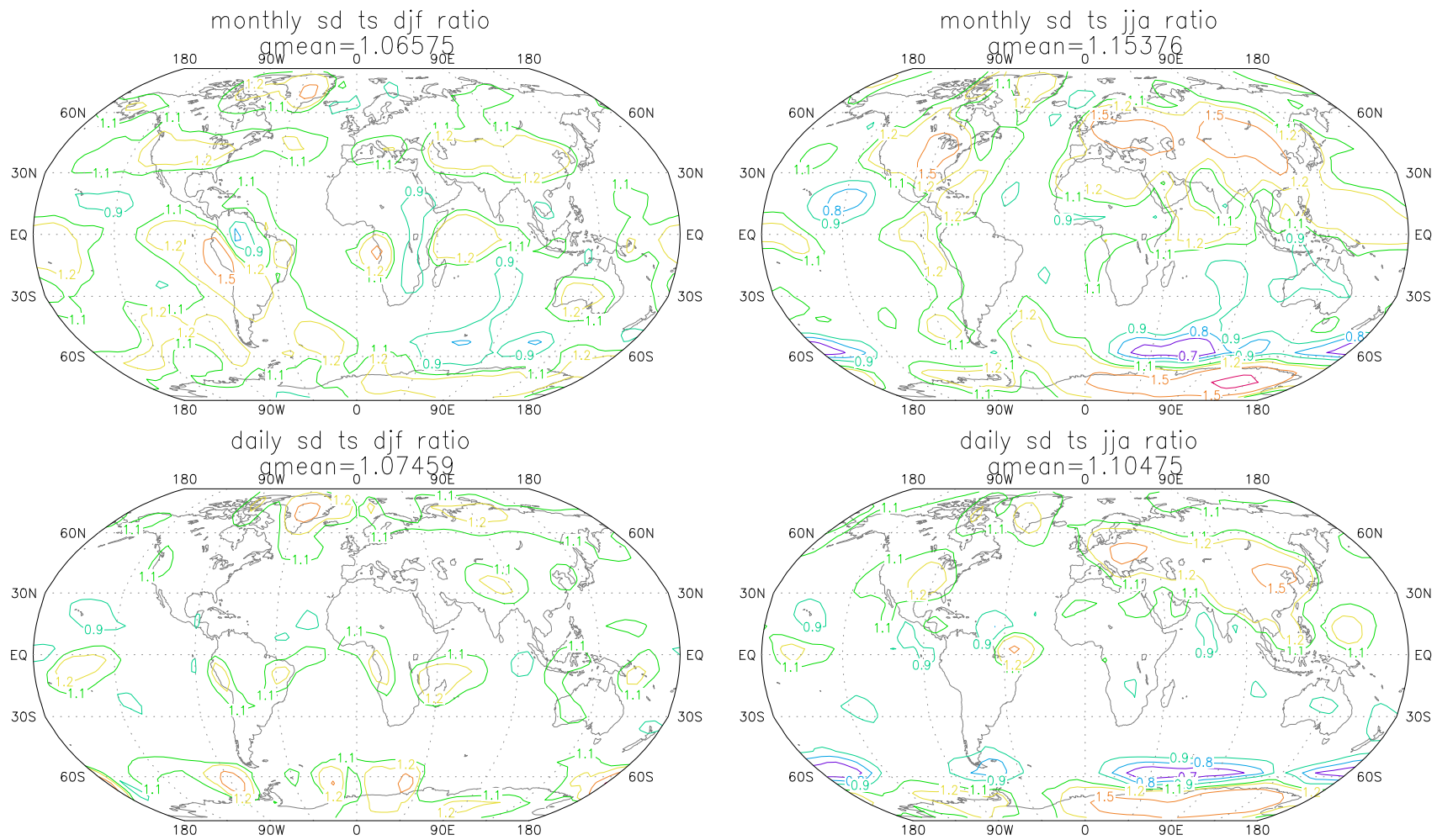


Figure 6: Interannual and daily surface temperature standard deviation ratios of the simulation with dynamical clouds and the simulation with prescribed climatological clouds for DJF (left panels) and JJA (right panels). The results are smoothed using a 9-point filter.

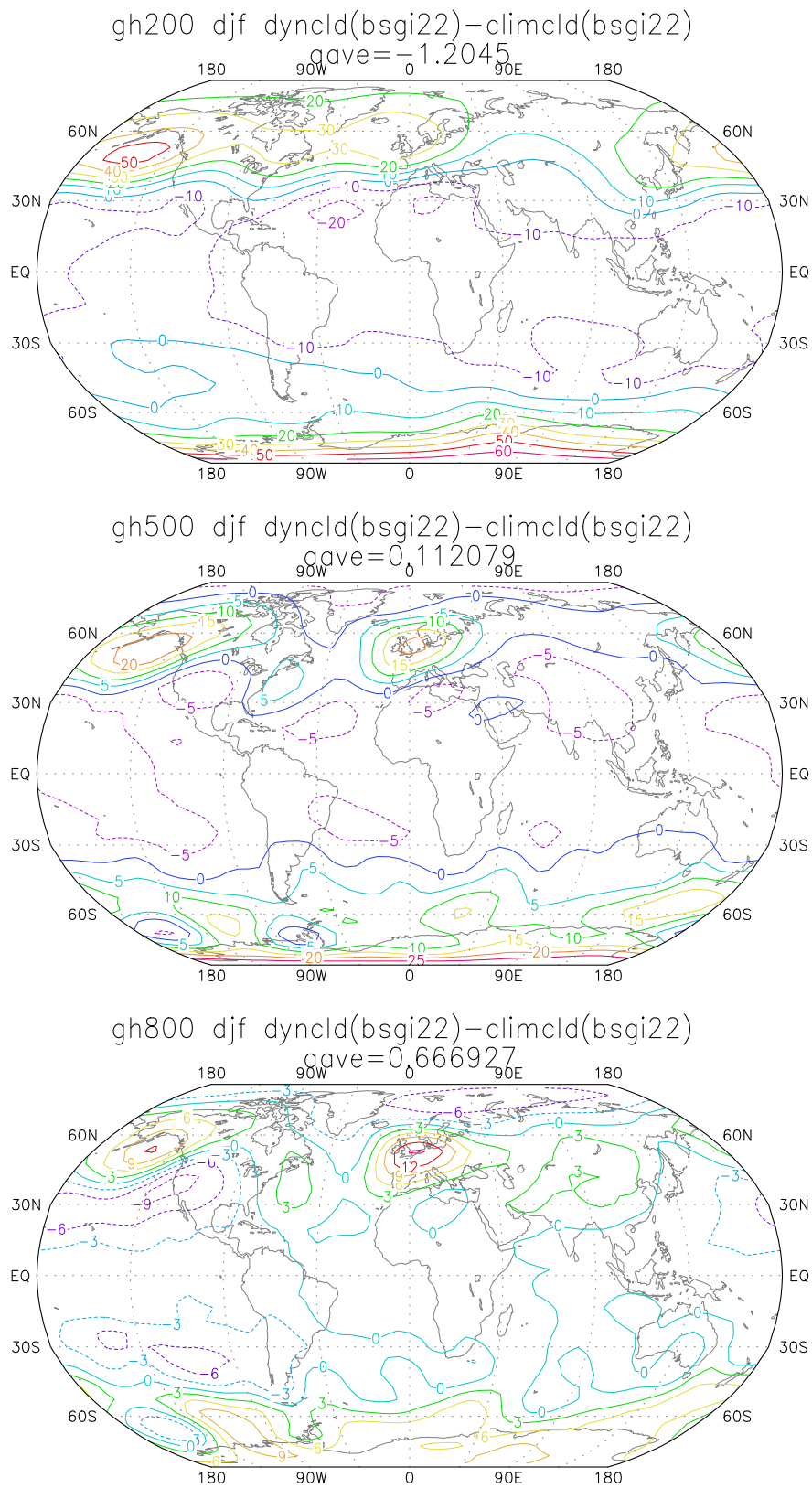


Figure 7: Geopotential height differences (m) between the simulation with dynamical clouds and the simulation with climatological clouds at 200, 500 and 800 hPa in DJF.

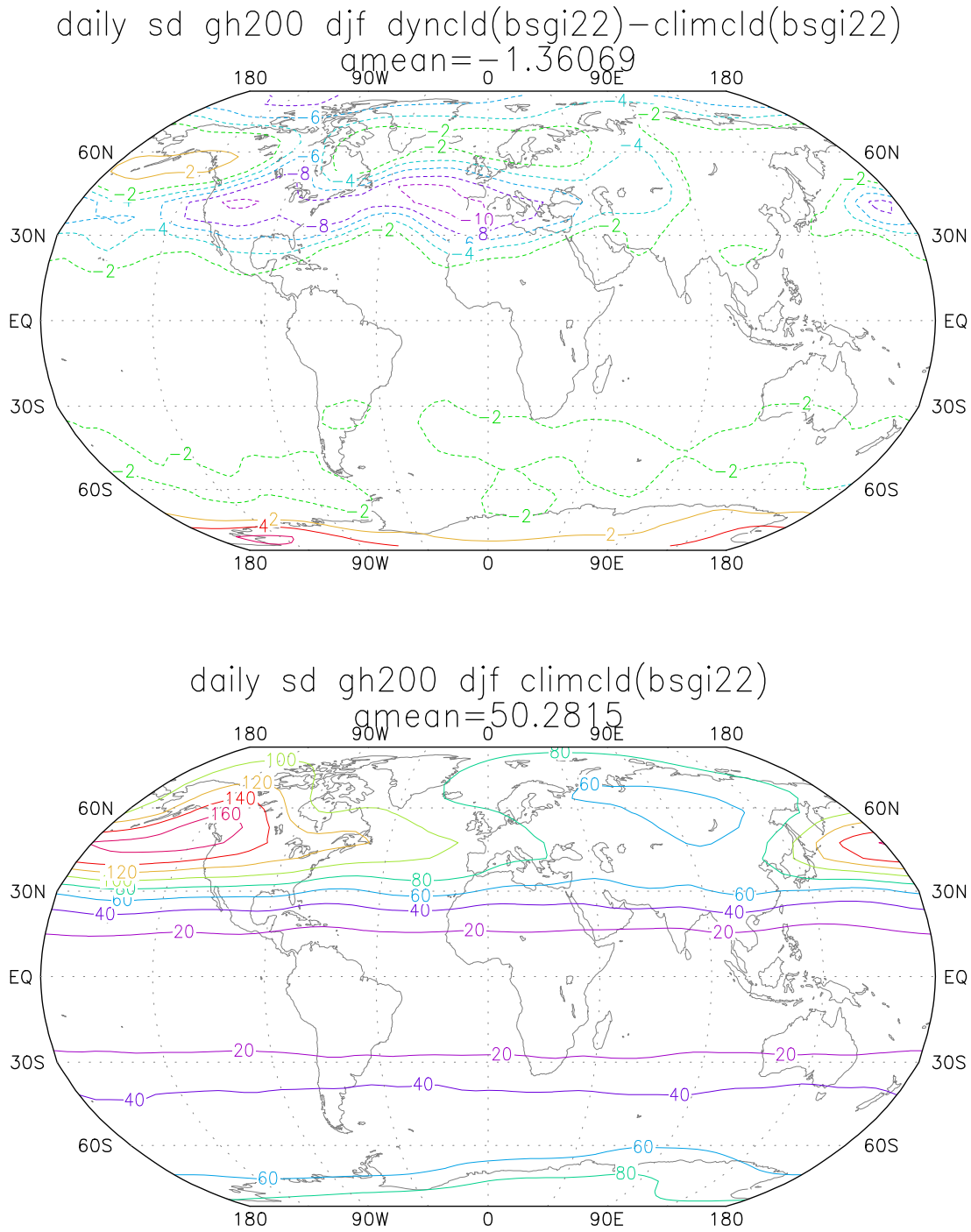


Figure 8: Difference in daily standard deviation of 200 hPa geopotential height (m) in the simulation with dynamical clouds and the simulation with climatological clouds (upper panel), and daily standard deviation of 200 hPa geopotential height (m) in the climatological cloud simulation (lower panel).

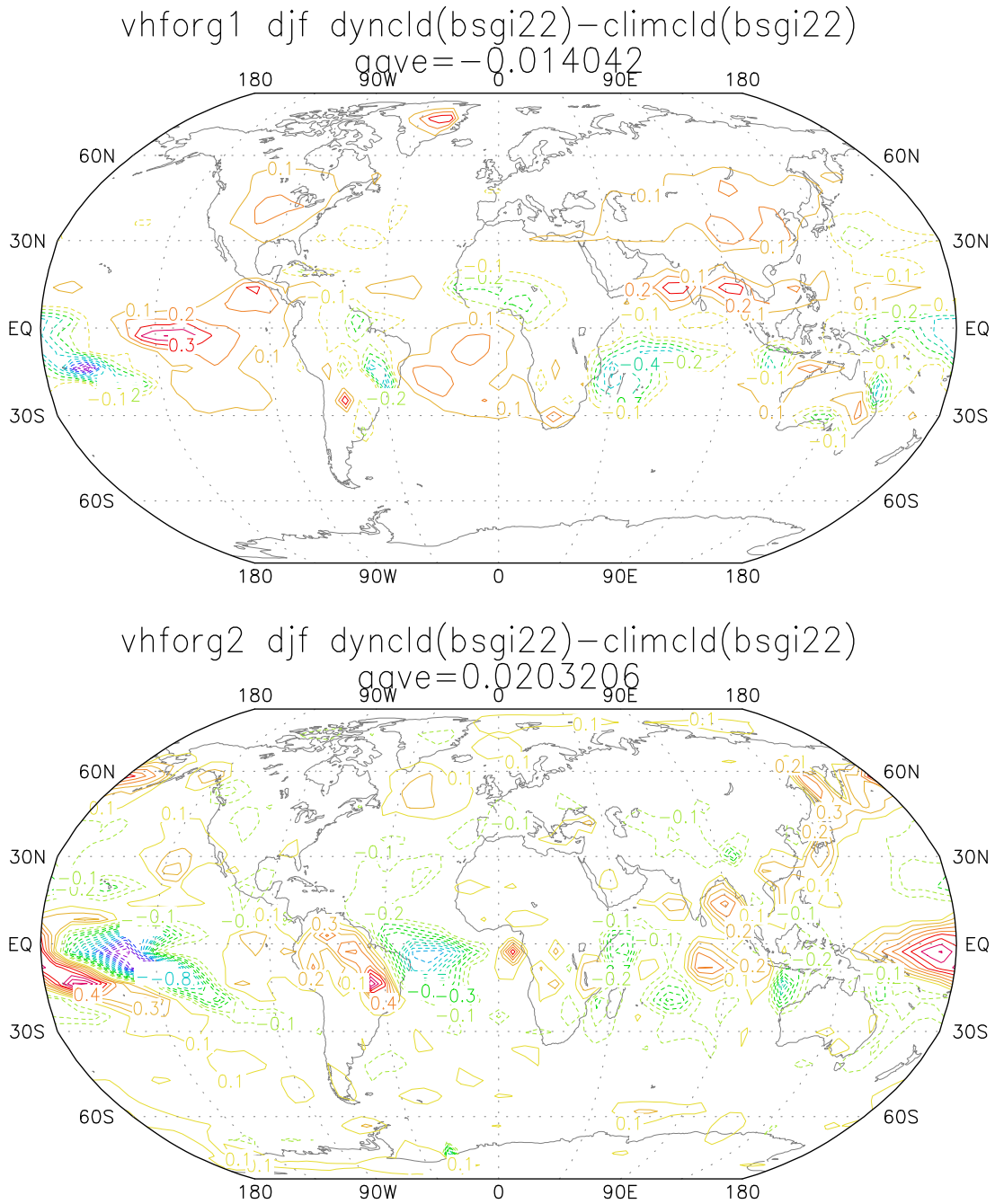


Figure 9: Diabatic heat differences ($^{\circ}\text{C day}^{-1}$) between the simulation with dynamical clouds and the simulation with climatological clouds for the layer between 500 and 200 hPa (upper panel) and the layer between 1000 and 500 hPa (lower panel) in DJF.

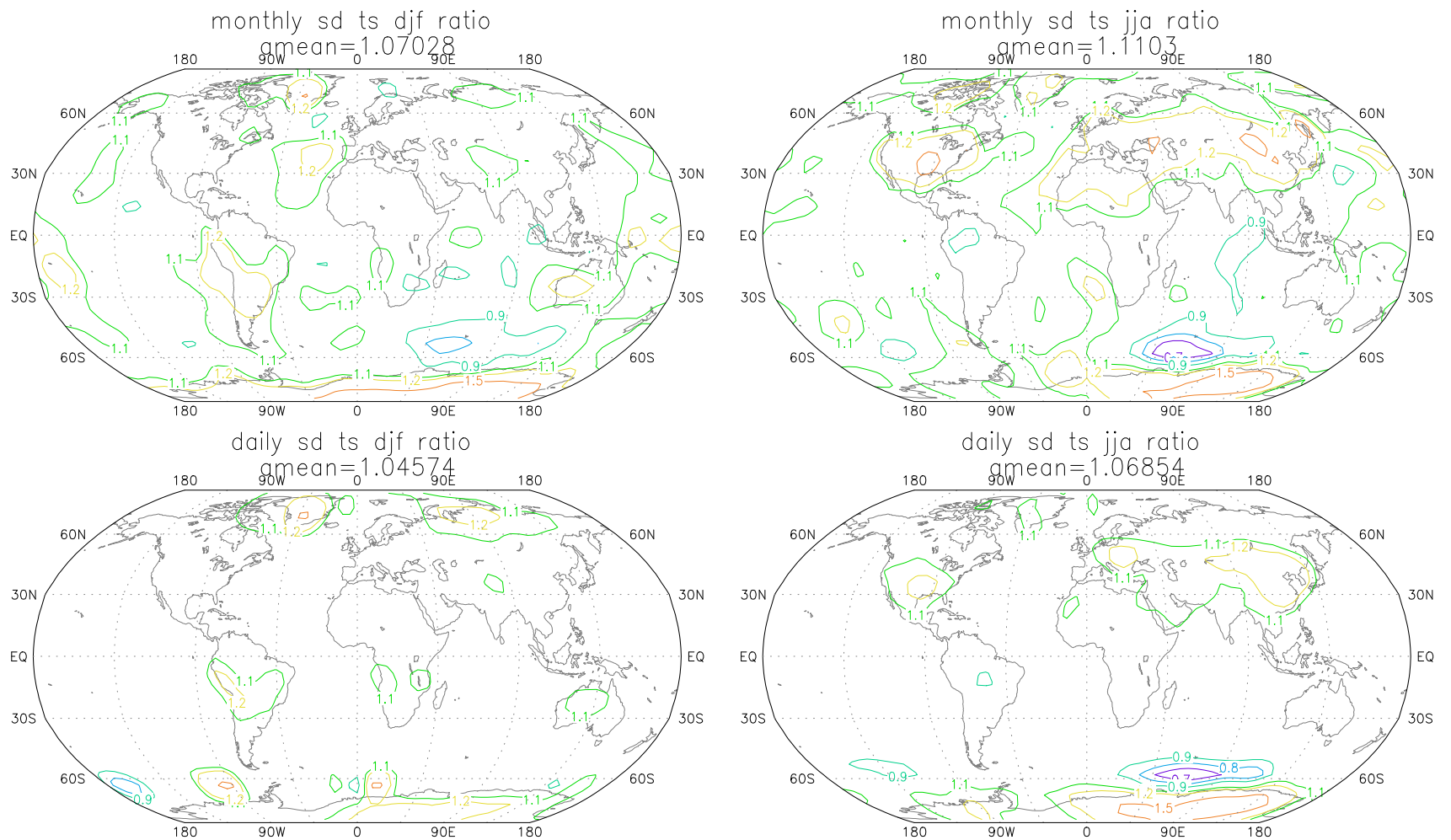


Figure 10: Interannual and daily surface temperature standard deviation ratios of the anomaly cloud simulation and the climatological cloud simulation for DJF (left panels) and JJA (right panels). The results are smoothed using a 9-point filter.

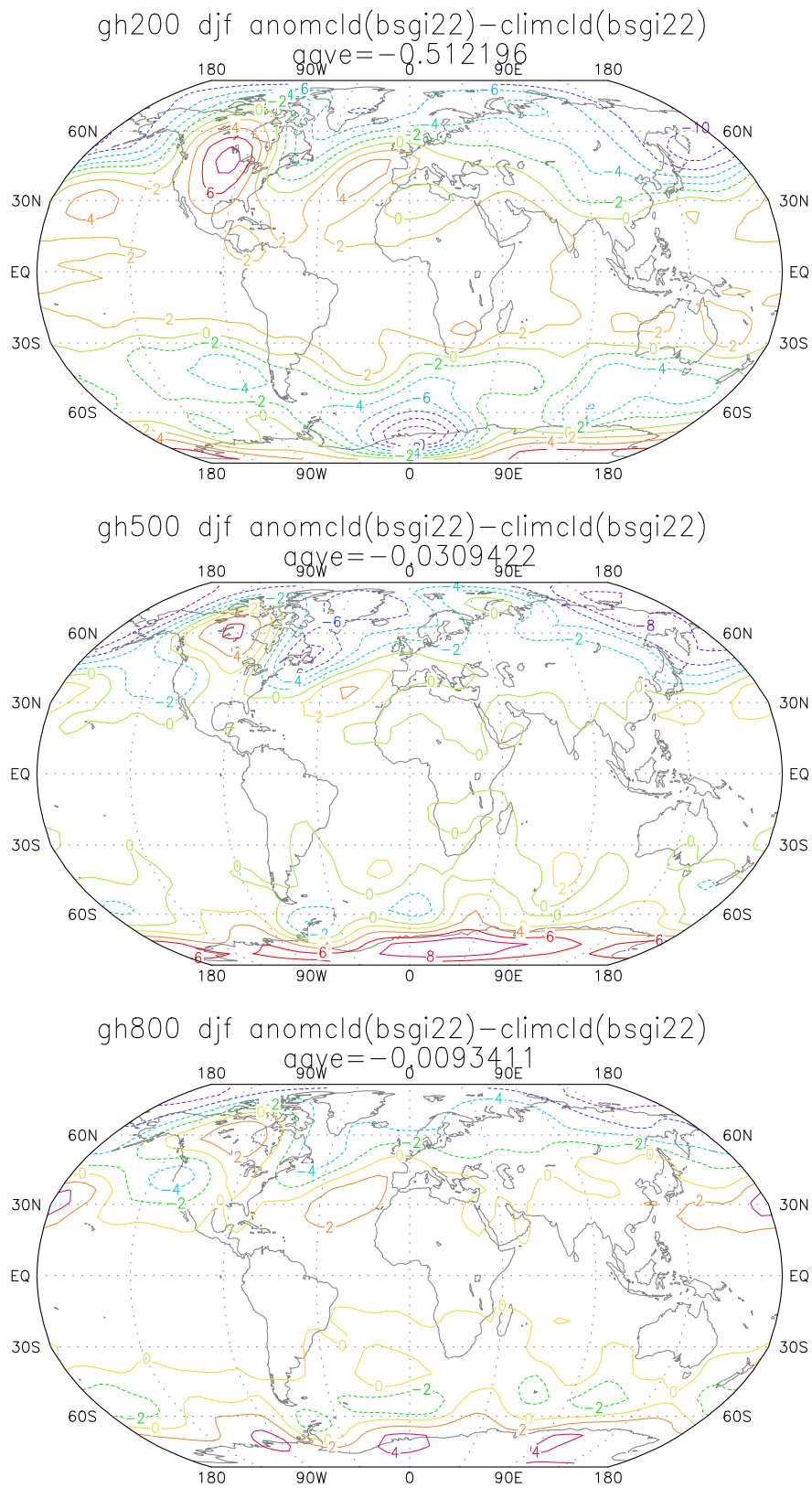


Figure 11: Geopotential height differences (m) between the simulation with anomaly clouds and the simulation with climatological clouds for 200, 500 and 800 hPa in DJF.

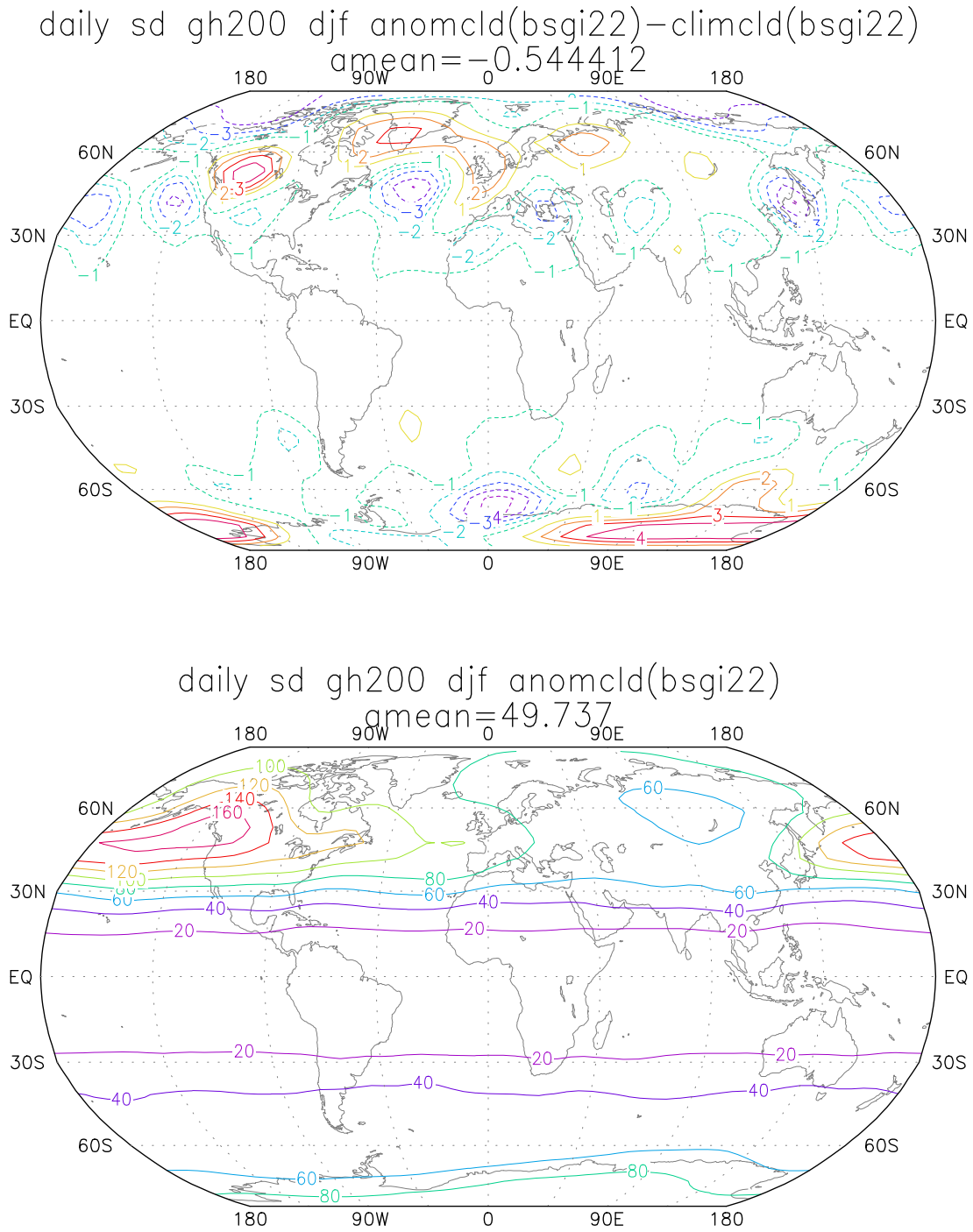


Figure 12: Difference in daily standard deviation of 200 hPa geopotential height (m) in the simulation with anomaly clouds and the simulation with climatological clouds (upper panel) and daily standard deviation of 200 hPa geopotential height (m) in the anomaly cloud simulation (lower panel).

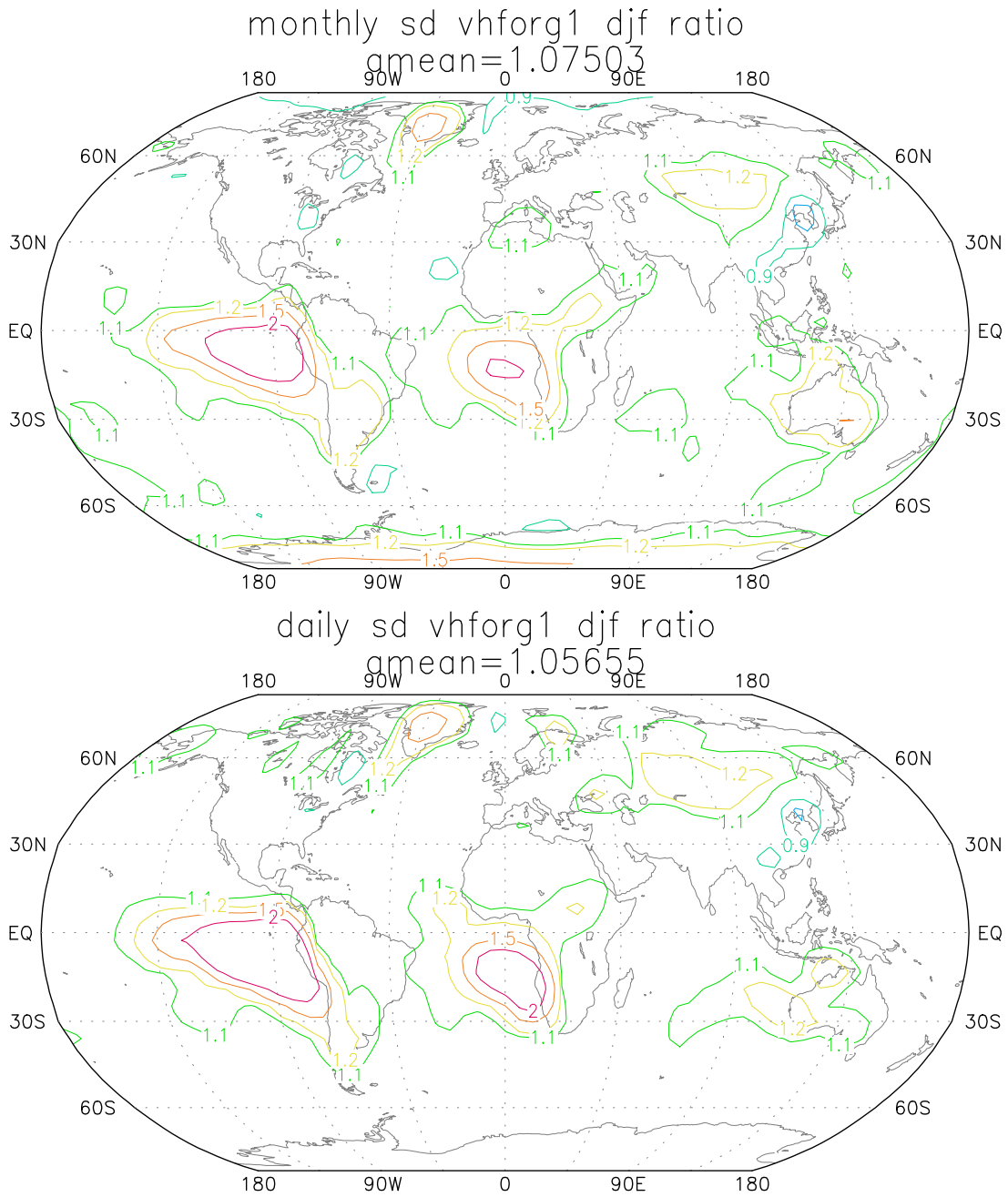


Figure 13: Ratios of standard deviations of diabatic heat in the simulation with anomaly clouds and the simulation with climatological clouds for the layer between 500 and 200 hPa in DJF. Upper panel: interannual standard deviations; bottom panel: daily standard deviations. The results are filtered using a 9-point smoother.

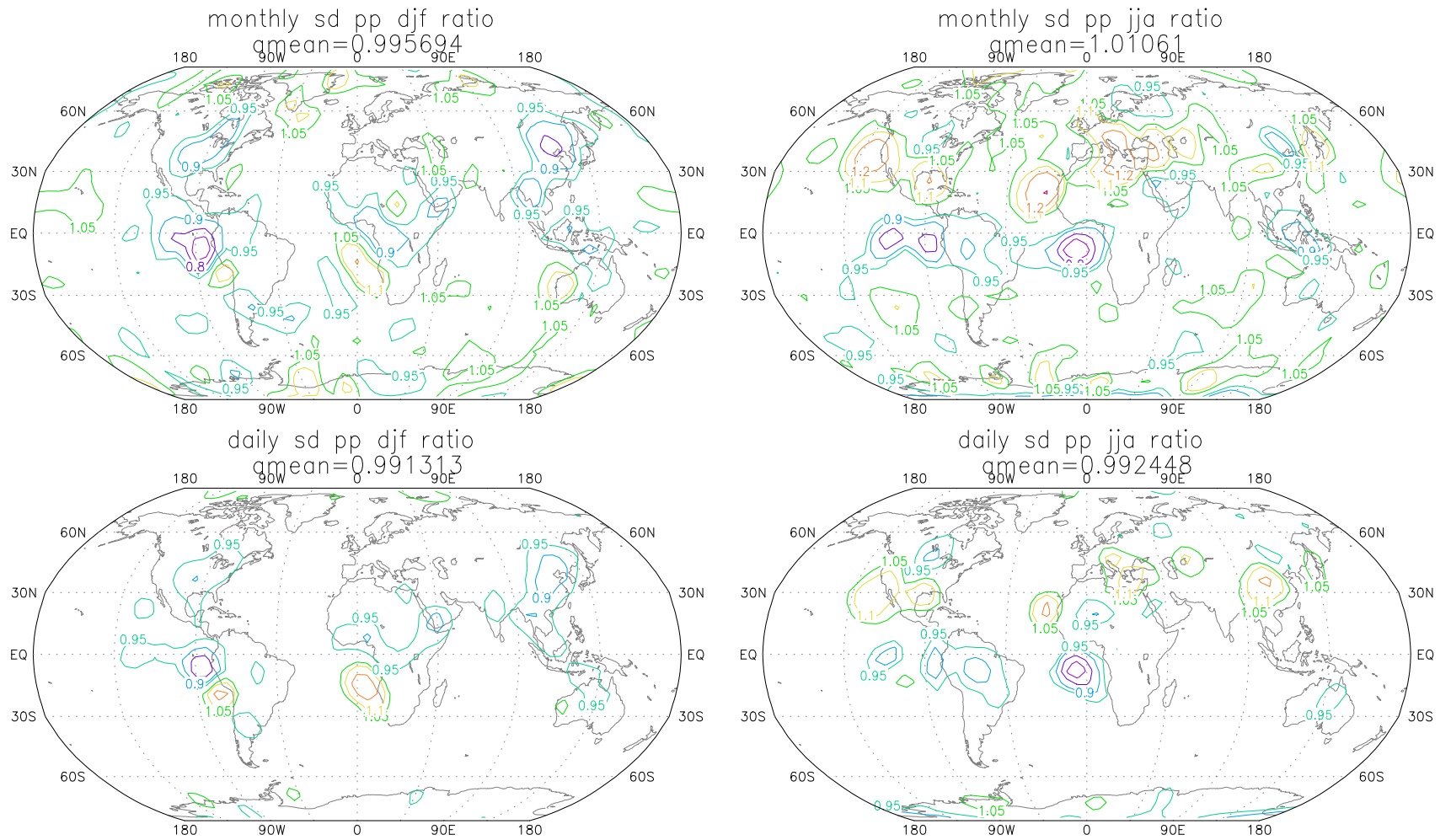


Figure 14: Interannual and daily precipitation standard deviation ratios of the anomaly cloud simulation and the climatological cloud simulation for DJF (left panels) and JJA (right panels). Precipitation consists of both large scale and convective precipitation. The results are smoothed using a 9-point filter.